Cocoa Pod Husk Carbon Family for Biogas Upgrading: Preliminary Assessment Using the Approximate Adsorption Performance Indicator

Khaled Abou Alfa, Diana C Meza-Sepulveda, Cyril Vaulot, Jean-Marc Le Meins, Camelia Matei Ghimbeu, Louise Tonini, Janneth A Cubillos, Laurent Moynault, Vincent Platel, Diego Paredes, et al.

Journal of Carbon Research

MDPI

Article

Cocoa Pod Husk Carbon Family for Biogas Upgrading: Preliminary Assessment Using the Approximate Adsorption Performance Indicator

Khaled Abou Alfa [1,*], Diana C. Meza-Sepulveda [2], Cyril Vaulot [3,4], Jean-Marc Le Meins [3,4], Camelia Matei Ghimbeu [3,4], Louise Tonini [1], Janneth A. Cubillos [5], Laurent Moynault [1], Vincent Platel [1], Diego Paredes [5] and Cecile Hort [1]

1 Laboratoire de Thermique, Energetique et Procedes-IPRA, EA1932, University of Pau and Pays de l'Adour/E2S UPPA, F-64000 Pau, France; louise.tonini@univ-tlse3.fr (L.T.); laurent.moynault@univ-pau.fr (L.M.); vincent.platel@univ-pau.fr (V.P.); cecile.hort@univ-pau.fr (C.H.)
2 Agroindustrial Development Group, Faculty of Agricultural Sciences and Agroindustry, Universidad Tecnologica de Pereira, Pereira 660004, Colombia; dcmeza@utp.edu.co
3 CNRS, Institut de Science des Matériaux de Mulhouse (IS2M) UMR 7361, Université de Haute-Alsace, F-68100 Mulhouse, France; cyril.vaulot@uha.fr (C.V.); camelia.ghimbeu@uha.fr (C.M.G.)
4 CNRS, Institut de Science des Matériaux de Mulhouse (IS2M) UMR 7361, Université de Strasbourg, F-67081 Strasbourg, France
5 Water and Sanitation Research Group, Faculty of Environmental Sciences, Universidad Tecnológica de Pereira, Pereira 660004, Colombia; diparede@utp.edu.co (D.P.)
* Correspondence: kaalfa@univ-pau.fr

Abstract: The preliminary selection of adsorbents for the separation of a gas mixture based on pure gas adsorption remains a critical challenge; thus, an approximate adsorption performance indicator (AAPI) was proposed for the initial evaluation of the adsorbents to separate the biogas main constituents (carbon dioxide/methane (CO_2/ CH_4)) by studying their pure gas adsorption. Three samples derived from cocoa pod husk (CPH), namely Cabosse-500 (pyrolyzed at 500 °C), Cabosse-700 (pyrolyzed at 700 °C), and Cabosse-A-700 (activated with CO_2 at 700 °C), were synthesized, characterized, and evaluated for the pure gases adsorption. This study presents an AAPI evaluation, which takes into account adsorption capacity, approximate selectivity, and heat of adsorption. Adsorption isotherms indicate the ability of the CPH family to selectively capture CO_2 over CH_4, as they have a high approximate selectivity (>1) thanks to their physical properties. Changing the pyrolysis temperature, activation methods, and varying the pressure can significantly change the choice of the most effective adsorbent; Cabosse-A-700 showed better performance than the other two in the low and high pressure range owing to its presence of micropores and mesopores, which enhances the CO_2 adsorption and therefore the AAPI.

Keywords: biogas; adsorption; activated biochar; approximate adsorption performance indicator; carbon dioxide; cocoa pod husk

check for updates

Citation: Abou Alfa, K.; Meza-Sepulveda, D.C.; Vaulot, C.; Le Meins, J.-M.; Ghimbeu, C.M.; Tonini, L.; Cubillos, J.A.; Moynault, L.; Platel, V.; Paredes, D.; et al. Cocoa Pod Husk Carbon Family for Biogas Upgrading: Preliminary Assessment Using the Approximate Adsorption Performance Indicator. *C* **2024**, *10*, 100. https://doi.org/10.3390/c10040100

Academic Editor: Sergey Mikhalovsky

Received: 8 October 2024
Revised: 15 November 2024
Accepted: 21 November 2024
Published: 29 November 2024

1. Introduction

Due to the growing cost, scarcity of energy and raw materials, and numerous environmental challenges stemming from human activities, alternatives to fossil fuels are urgently needed. One promising alternative is raw biomass, which can be converted into a renewable energy source in the form of biogas—a practical solution to global energy and environmental concerns that has seen growing application in recent years [1]. Biogas is generated by the anaerobic digestion of complex organic materials. Its composition varies depending on the type of raw biomass used and the specific conditions of the anaerobic digestion process. It consists primary of methane (40–75% v/v) and carbon dioxide (CO_2) (25–55% v/v) with trace amounts of other gases such as hydrogen sulfide (H_2S), ammonia

(NH_3), water vapor, siloxanes, halogenated hydrocarbons, etc. [2]. Biogas is a valuable fuel that can be used for direct heating, internal combustion engines, and, with improved efficiency, in cogeneration for electricity production. It is an environmentally friendly source, considered a promising way to meet global energy demands and minimize environmental impact with lower CO_2 levels, in conformity with EU directives on climate change [3]. Its upgrading (separation of CO_2 content) is crucial to meet quality standards for various applications, such as injection into natural gas grids or as vehicle fuel [4].

Existing CO_2 separation technologies from CH_4 each have specific limitations. Water scrubbers, while effective, require huge amount of fresh water and are less efficient at lower temperatures and pressures. Membrane systems often require multiple stages to achieve high purity, which increases both complexity and cost, and the membranes themselves can degrade over time. Chemical scrubbers, although efficient, are energy-intensive due to the need for solvent regeneration. They aso pose environmental and health risks. Organic physical scrubbers face similar challenges, such as high energy demands and environmental concerns. Cryogenic separation, despite its ability to achieve high purity, is extremely costly and energy-intensive due to the required cooling process [5–8]. Given these drawbacks, pressure swing adsorption (PSA) has emerged as a more attractive option due to its high removal efficiency, low energy needs, simple operation, and design flexibility. PSA operates based on the adsorption of CO_2 onto the adsorbent surface under varying pressure, making physical and chemical interactions pivotal for effective separation [9].

Various physical materials are utilized as adsorbents in PSA. Biomass residues undergo pyrolysis to produce biochar and subsequent activation to generate activated biochar, gaining attention for their sustainability and alignment with circular economy principles. They show promise in CO_2 capture due to their tunability, availability of precursors, waste valorization, low cost, excellent chemical and thermal stability [10–12]. They differ in production methods, surface characteristics, and availability, and can be engineered for enhanced CO_2 separation from CH_4 by controlling surface area, pore size distribution, and surface functional groups [13,14]. Their hydrophobic nature enables effective CO_2 capture, even in the presence of trace impurities such as moisture [4].

Cocoa cultivation has been evaluated as a promising alternative for biodiversity conservation due to its agroforestry approach, utilizing tree canopies for natural shade. West Africa, including Ivory Coast, Ghana, Cameroon, and Nigeria, stands as the world's largest cocoa producer, yet expansion faces hurdles like forest scarcity and protection measures [15]. Cocoa is one of the fastest-growing crops in the world, with an estimated world production of 5024 million tons during the 2020–2021 harvest [16]. The substantial residual biomass generated, comprising 79% to 90% of the total cocoa pod husk (CPH), poses environmental concerns and economic losses due to poor management and diseases such as *Phytophthora* spp. [17]. However, this biomass can be transformed into value-added bioproducts such as biofilms, biochars, activated biochar, and biofuels, offering avenues for sustainable utilization and waste reduction [15,18–20].

Different investigations have explored the use of CPH and other waste materials in regions with high cocoa production, highlighting a direct link between increased production, greater waste generation, and the need to identify useful applications for this waste [21]. The ash content in CPH typically ranges from 8% to 16% [18,22], and the most prevalent inorganic element is potassium (K), which accounts for approximately 50% of the ash content. These inorganic minerals in biochar can negatively affect its pores, since the specific surface area value is less than 100 $m^2\ g^{-1}$ at higher pyrolysis temperatures [23]. However, CPH activation with CO_2 revealed that increasing the activation temperature from 600 to 900 °C resulted in improved textural properties, with the BET surface area increasing from 352 to 817.1 $m^2\ g^{-1}$ and the micropore volume from 0.156 to 0.368 $cm^3\ g^{-1}$ [24]. Trending research highlights CPH as a promising energy source for treating pollutants in the aqueous phase. For instance, an AC was derived by activating a CPH-based biochar with H_3PO_4 for Lumefantrine removal, an antimalarial drug. Araoye et al. [25] demonstrated a yield of

90.9% at an initial drug concentration of 20 mg L^{-1}, attributed to the high carbon content, presence of hydroxyl functional groups, and cylindrical pores on the AC surface.

In addition, CPH has been observed as a precursor for developing adsorbents for water treatment, achieving a removal efficiency of over 90% of heavy metals and dyes [26]. Furthermore, an acid-washed biochar based on CPH was considered an effective adsorbent for removing cationic compounds from aqueous solution, owing to its microporous characteristics, with a BET surface area of 342 m^2 g^{-1} and a total pore volume of approximately 0.20 cm^3 g^{-1} [18]. Additionally, CPH carbonization at 500 °C for 50 min has been suggested as a potentially useful source due to its composition of various organic compounds, including ketones, carboxylic acids, aldehydes, furans, heterocyclic aromatics, alkylbenzenes, phenols, and benzenediols [27].

In this context, this first innovative study focuses on the use of CPH as a raw biomass for producing biochars and activated biochar tailored for CO_2 and CH_4 capture. The distinctive aspect of our research lies in addressing the gap in the existing literature, as no prior studies have addressed the use of CPH for upgrading biogas. The primary objective of this study is to evaluate and compare the adsorption performance of a CPH family using a new indicator called the "Approximate Adsorption Performance Indicator" based on pure gases CO_2 and CH_4 considering three key adsorption factors: heat of adsorption, working capacity, and approximate selectivity. To achieve this, a comprehensive physicochemical analysis was carried out using various analytical methods to delve into the adsorption characteristics. Techniques employed included thermogravimetric analysis (TGA), scanning electron microscopy (SEM), energy dispersive X-ray (EDX), X-ray diffraction (XRD), and gas adsorption analysis.

2. Materials and Methods

2.1. Materials

2.1.1. Raw Biomass

The sampling unit is located in Marsella-Risaralda in Colombia, Gilberto Peláez farm of the National Federation of Cocoa Growers FEDECACAO. The selection process was based on stable production over the past year, ensuring that the cocoa clones were properly identified and not crossbred, as well as being free from phytosanitary diseases. The CCN51 clone of Ecuadorian origin was chosen based on criteria of the state of maturity of the cob and higher population density in the department of Risaralda, Colombia. More information about its preparation and characteristics is presented in Appendix A.1.

2.1.2. Biochars and Activated Biochar Preparation

Three samples were prepared for evaluation and comparison: Cabosse-500 and Cabosse-700, biochars pyrolyzed at 500 °C and 700 °C, respectively, and Cabosse-A-700, an activated biochar produced at 700 °C. These temperatures were selected based on the optimal temperature ranges for obtaining optimal textural properties [28,29]. Initially, raw CPH on a dry base underwent pyrolysis at 500 °C in an oxygen-limited environment to produce Cabosse-500 with a 63.3% mass loss (Figure 1). Prior to the experiment, the biomass basket underwent a 60 min purge with N_2 at a flow rate of 13.2 g min^{-1} to create an inert atmosphere, preventing unwanted reactions like oxidation during high-temperature treatment. Then, the furnace temperature was raised at a rate of 10 °C min^{-1} until reaching the desired pyrolysis temperature of 500 °C, which was maintained for 60 min. This pyrolysis was conducted at the University of Pau and Pays de l'Adour. Cabosse-500 was then subjected to a pyrolysis process at 700 °C in a cylindrical reactor at the Université de Haute-Alsace. The reactor tube was purged with Argon for 30 min and then heated to 700 °C at a rate of 10 L h^{-1} for 60 min to obtain Cabosse-700 with a mass loss of 26.33%. The choice of two different protective gases was due to the resources and protocols available at each laboratory. After several attempts, an activation of Cabosse-700 with CO_2 at a temperature of 700 °C for 1 h at a CO_2 flow rate of 6 L h^{-1} yielded Cabosse-A-700, with a mass loss of 8.6% (more information in Appendix A.2).

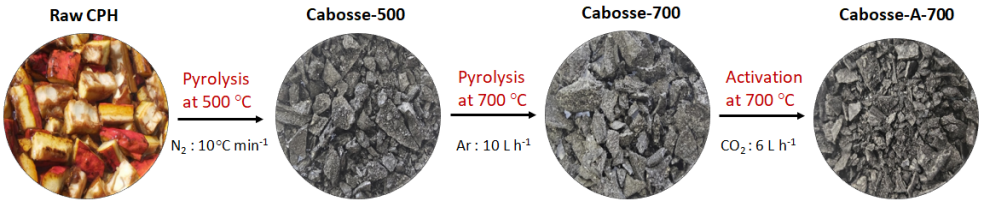

Figure 1. Biochars and activated biochar preparation.

2.2. Physicochemical Characterization of the CPH Family

2.2.1. Scanning Electron Microscope (SEM) and Energy Dispersive X-Ray (EDX)

The carbon morphology of the CPH family was observed by SEM analysis. Micrographs were acquired with a FEI Quanta 400 scanning electron microscope with a high-resolution low-vacuum field emission gun (FEG). This microscope was also equipped with a JED 2300 detector for energy-dispersive X-ray (EDX) spectroscopy to determine the quantitative chemical composition of materials. EDX was chosen for its ability to provide localized elemental data, which is crucial for analyzing specific micro-regions of the CPH samples. However, it does not provide bulk elemental analysis. Several EDX acquisitions were performed in large areas, and the average values are presented.

2.2.2. X-Ray Powder Diffraction (XRD) Technique

X-ray diffraction is often the most common technique to obtain structural information about crystalline materials. The measurements were performed using a Bruker D8 Advanced diffractometer with Bragg–Brentano θ-θ geometry equipped with a LynxEye XE-T high-resolution energy-dispersive one-dimensional (1D) detector (Cu K α1,2). Data collection was performed in the 10–90° 2θ domain,with a step size of 0.015° 2θ and a total acquisition time of 1 h.

2.2.3. Thermogravimetric Analysis (TGA)

TGA is a high-performance thermal technique used to measure the weight changes in a sample as a function of temperature in a controlled environment. TGA analysis was carried out using METTLER TOLEDO TGA 851e. The process involved heating the raw biomass from room temperature to 107 °C at a rate of 5 °C min^{-1} under N_2, holding it for 15 min, then ramping the temperature from 110 °C to 950 °C at a rate of 5 °C min^{-1} and maintaining it for 7 min. Subsequently, the temperature was lowered to 750 °C at a rate of 5 °C min^{-1} under N_2, followed by a switch to air flow and a 15 min hold. However, the weight loss of the biochars and activated biochar was obtained by heating the samples up to 900 °C at a rate of 5 °C min^{-1} under N_2 and air (100 mL min^{-1}) to obtain the thermal decomposition profiles at different temperatures and mass loss [30].

2.2.4. N_2 and CO_2 Physisorption

N_2 physisorption tests were conducted at 77 K on a Micromeritics ASAP 2420 instrument and CO_2 tests were carried out at 273 K on a Micromeritics ASAP 2020 instrument. The CPH family were first out-gassed under vacuum for 12 h at 300 °C on the degassing port and then for an additional 2 h treatment on the analysis port to empty the porosity before analysis. The determination of equivalent Brunauer–Emmett–Teller (BET)-specific surface areas involved examining linear plots in the relative pressure ranges (P/P_0) of 0.01–0.3 for N_2 and CO_2, and the precise pressure ranges were adapted for each sample thanks to Rouquerol's curve, the correlation coefficient of the BET transform ($R_2 > 0.9999$), and the positive value of the BET constant "C". The total pore volume (V_t) was determined using the N_2 adsorption at P/P_0 of 0.99, and the Dubinin–Radushkevich model was applied to calculate the micropore volume (V_{micro}) within the relative pressure range of 10^{-4} and 10^{-2}. Then, the mesopore (V_{meso}) volume was calculated by the difference between total V_t and V_{micro} [30].

2.3. Experimental Setup for Investigating Adsorption Characteristics

2.3.1. High-Pressure Differential Scanning Calorimeter

The heat of CO_2 adsorption into the biochars and activated biochar was determined using a high-pressure differential scanning calorimeter, specifically the micro DSC VII from Setaram. The calorimeter block consists of two gas-tight high-pressure cells, the adsorption and reference cells (Figure 2), both made of stainless steel with a volume of 1 cm^3. Samples of approximately 70 mg are carefully weighed before placement into the measurement cell. To remove any residual fluids in the system, a regeneration process is performed, which involves subjecting the sample to vacuum (10^{-2} Pa) through the gas panel and heating at 373 K for 24 h. Subsequently, the furnace, including both cells, is cooled from 373 K to 303 K at a rate of 1 K min^{-1}. The system is stabilized at 303 K throughout the adsorption process to ensure uniform temperature distribution and heat flow signal stabilization. Then, a quantity of pure CO_2 is introduced and regulated through the gas panel until the pressure in the system is stabilized, as previously described by Abou Alfa et al. [31].

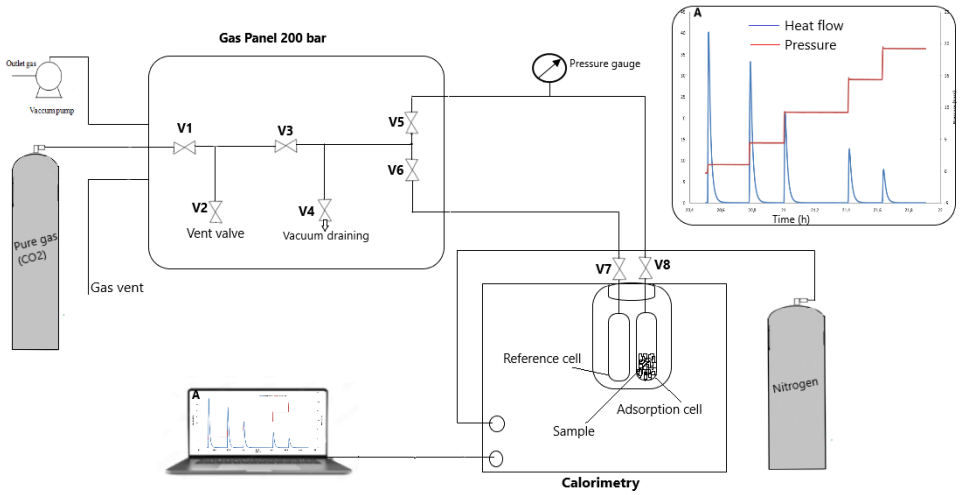

Figure 2. Schematic of the calorimeter "micro DSC VII".

2.3.2. Gas Adsorption Isotherm

The apparatus used to obtain the pure gas adsorption isotherms is a homemade high-pressure manometric setup represented schematically in Figure 3. The procedure steps were already published [32,33] and are presented in Appendix A.3. The adsorption capacities of gases were determined using equations presented in the literature [34].

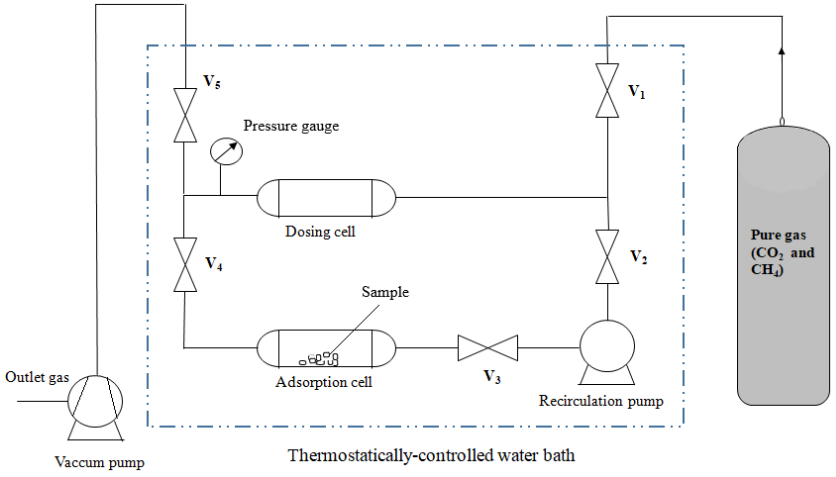

Figure 3. Schematic representation of a high-pressure homemade manometric device.

2.4. Approximate Adsorption Performance Indicator

The Approximate Adsorption Performance Indicator (AAPI) offers several advantages when evaluating adsorbent performance by integrating key factors such as selectivity, adsorption capacity, and heat of adsorption into a single, comprehensive metric. This approach simplifies the complexity of performance evaluation and is particularly valuable in tailoring assessments to different industrial needs. Since the separation of a binary gas mixture using adsorbents relies on these three critical factors, the AAPI provides a way to combine them with varying relative importance based on the specific objectives of the separation process, such as biogas purification or upgrading. This adaptability makes the AAPI particularly valuable in tailoring assessments to different industrial needs. The AAPI concept was adapted from an indicator called the "Adsorption Performance Indicator", which is used for evaluating adsorbents for a mixture of gases, as proposed by Wiersum et al. [35].

This study focused on the adsorption of pure gases rather than the gas mixtures. Therefore, the calculated CO_2/ CH_4 selectivity was the approximate selectivity; refer to literature [36,37]. This approximate selectivity provides insight into which samples might be promising adsorbents for the final comparison. The approximate selectivity was determined using the following equation:

$$S_{CO_2/CH_4} = \frac{n_{exc,CO_2}}{n_{exc,CH_4}} \quad (1)$$

where n_{exc,CO_2} and n_{exc,CH_4} (mol kg^{-1}) are the excess adsorbed amounts of CO_2 and CH_4, respectively.

The adsorption indicator calculated was the Approximate Adsorption Performance Indicator (AAPI), which is related to the approximate selectivity and the adsorption capacity of the stronger adsorbate component. Then, the AAPI can be written as follows:

$$AAPI = \frac{(\tilde{S}_{1/2} - 1)^A WC_1^B}{|\Delta H_{ads,1}|^C} \quad (2)$$

In Equation (2), $\tilde{S}_{1/2}$ is the approximate selectivity of Component 1 over Component 2, WC_1 is the working capacity of the stronger adsorbate Component 1, and $\Delta H_{ads,1}$ is the heat of adsorption of Component 1 which takes place in the denominator of the relation because it is detrimental to the process performance. A, B, and C are the exponents of the approximate selectivity, the working capacity, and the heat of adsorption, respectively. These exponents can be adjusted to offer the relative importance of each one according to the objectives of the separation process [35].

3. Results and Discussion

3.1. CPH Family Characterization

3.1.1. SEM Analysis

The morphology of the CPH family, Cabosse-700 and Cabosse-A-700, was analyzed using SEM at different magnification scales (500 µm, 200 µm, and 100 µm) (see Figure 4). There were significant differences in the morphological shape between the two samples; SEM images of Cabosse-700 (a) showed a rigid structure with the absence of pores. On the other hand, Cabosse-A-700 revealed a breakdown of the rigid structure, resulting in a more porous and textured surface. Although the BET offers indication of micropore formation, SEM indicates the formation of larger pores, macropores. Cabosse-A-700 exhibited a higher BET surface area of 97 m^2 g^{-1} compared to Cabosse-700, which had a surface area of only 4 m^2 g^{-1} (Table 1). Cabosse-A-700 exhibited many honey-combed pores distributed on the surface with more cracking and a higher presence of pores. Similar observations were shown in a study conducted on CPH by comparing SEM images of its pyrolysis and activation [38]. These characteristics of the AC suggest that gas molecules can diffuse better and lead to improved adsorption efficiency [39].

Table 1. Textural and chemical characteristics of the cabosse family.

Textural Properties	Raw Biomass	Cabosse-500	Cabosse-700	Cabosse-A-700
S_{BET} (CO_2) (m^2 g^{-1})	n.a	n.a	41	112
S_{BET} (N_2) (m^2 g^{-1})	n.a	3	4	97
V_t (cm^3 g^{-1})	n.a	0.0002	0.003	0.06
V_{micro} (cm^3 g^{-1})	n.a	0	0	0.011
V_{meso} (cm^3 g^{-1})	n.a	0.0002	0.003	0.049
Proximate analysis (wt.%)				
Moisture	10.1	6.6	1.1	n.a
Volatiles	62.6	31.7	21.3	n.a
Fixed carbon	19.3	44.4	56.7	n.a
Ash	8	17.3	20.9	26
Elemental analysis (wt.%)				
Carbon	n.a	44.2	44.1	24.2
Oxygen	n.a	30.5	33.1	33.2
Potassium	n.a	19.9	18.1	34.6
Aluminum	n.a	0.4	-	-
Calcium	n.a	1.8	1.7	2.1
Magnesium	n.a	1.1	1.2	1.8
Sodium	n.a	0.4	0.6	1.1
Chlorine	n.a	0.7	0.4	1.8
Sulfur	n.a	0.5	0.4	0.7
Phosphorus	n.a	0.5	0.3	0.5
Copper	n.a	-	0.1	-

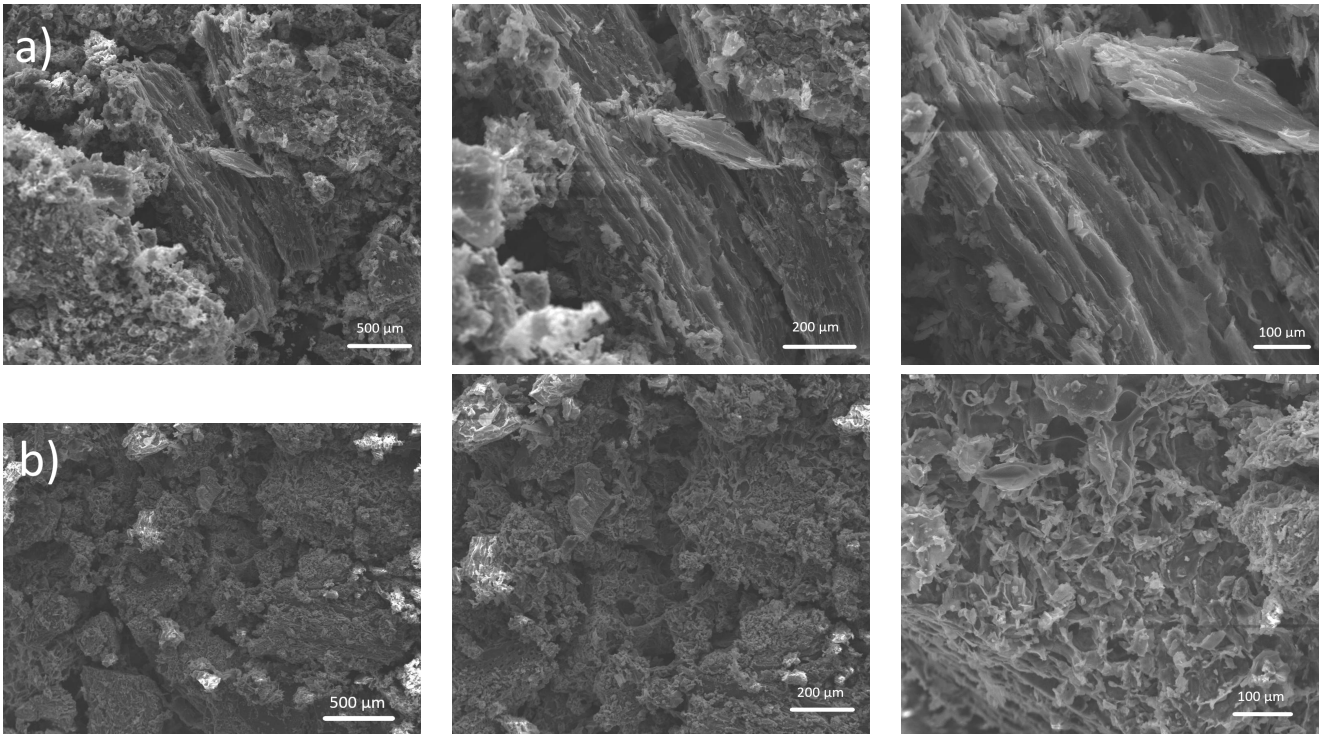

Figure 4. Morphology of the CPH family obtained by SEM at different magnification scales (500 µm, 200 µm, and 100 µm) of (**a**) Cabosse-700 and (**b**) Cabosse-A-700.

3.1.2. EDX Analysis

The elemental analysis by EDX, as shown in Table 1, indicated the presence of carbon (C), oxygen (O), and potassium (K) as the main elements, as well as minor elements such as calcium (Ca), magnesium (Mg), etc. The CPH family is rich in carbon and oxygen, typical for chars converted from agricultural residuals [40]. The increase in the carbonization temperature results in variations in the resulting biochar's chemical composition, as confirmed by the literature [18,41]. Cabosse-500 exhibits a carbon content of 44.2 wt.%, which remains approximately constant after pyrolysis at 700 °C (44.1 wt.%) (Table 1). These findings suggest that the small difference in the pyrolysis temperature has a limited impact on the carbon content, and the volatile carbon was already removed after pyrolysis at 500 °C. However, a substantial reduction in carbon content to a value of 24.2 wt.% was observed in Cabosse-A-700. During this activation, the adsorbent experienced a mass loss of 8.6%, corresponding to a yield of 91.4%, meaning that 91.4% of the original Cabosse-700 material was retained after activation. The carbon content decreased from 44.1% in Cabosse-700 to 24.2% in Cabosse-A-700. Consequently, 50.1% of the original carbon content in Cabosse-700 was retained in Cabosse-A-700. This reduction in carbon content reflects the activation process, which oxidizes some of the carbon to enhance the material's porosity and surface area. Despite the reduction in carbon, the high yield of 91.4% indicates that most of the original biomass was preserved, making Cabosse-A-700 an effective adsorbent with improved characteristics due to its activation.

Regarding the oxygen content in the CPH family, Cabosse-500 has an oxygen level of 30.5 wt.%, which increases slightly to 33.1 wt.% in Cabosse-700; this could be due to the thermal decomposition of organic matter at higher pyrolysis temperatures, as confirmed by the TGA analysis (Table 1), which results in the formation or retention of oxygen-containing functional groups such as carbonyl and hydroxyl [18]. Interestingly, the oxygen level in Cabosse-A-700 (33.2 wt.%) is kept constant compared to Cabosse-700 (33.1 wt.%). Thus, the activation stage at 700 °C likely concentrates on eliminating volatile components without introducing additional oxygen groups. However, O might come from the inorganics (oxides carbonates, etc.), as sustained by XRD analysis (Figure 5). Their oxidation state/form can change during pyrolysis and activation, inducing different O contents.

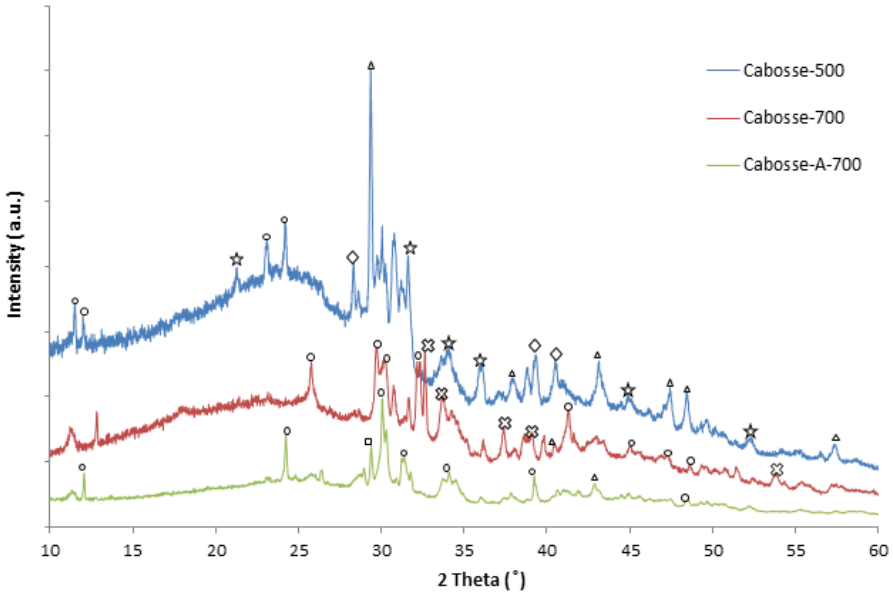

Figure 5. XRD analysis of the CPH family. ○ K_2CO_3, □ SiO_2, △ $CaCO_3$, ☆ K_2SO_4, ◇ ClK, and × $MgCO_3$.

However, the main inorganic element in the CPH family was potassium (K), ranging from 34.6 wt.% to 18.1 wt.% (Table 1), in the form of K_2CO_3 and K_2SO_4 (Figure 5). A similar observation was reported in recent studies conducted on CPH, where it was shown that potassium is responsible for approximately 17.28% of a CPH pyrolyzed at 800 °C [18]. Cabosse-500 has a high potassium amount of 19.9 wt.%, which remains rather constant, i.e., 18.1 wt.% when pyrolyzed at 700 °C. The activation of biochar with CO_2 at 700 °C results in a significant increase in potassium content to 34.6 wt.%, which can be confirmed by the increase in the ash content in TGA analysis, probably because the activation selectively removes other carbon components or enhances potassium retention in the biochar matrix.

3.1.3. XRD Analysis

In comparison to samples produced from other feedstocks, the CPH family exhibited high crystalline phases due to the presence of ash (see Table 1) [42–44]. Pyrolysis and activation processes have affected the crystal structure of the material, as shown by the shifts in the peak positions and the changes in the peak intensities (Figure 5). At lower pyrolysis temperatures (500 °C), the XRD pattern has a large diffuse peak at 2θ = 20–28°, indicating the existence of turbotratic carbon, a characteristic of low thermal treated carbon material [45]; this peak is lower in Cabosse-700 because a significant amount of biomass can undergo thermal degradation. However, the XRD patterns show that Cabosse-A-700 has sharper and higher intensity peaks than Cabosse-500 and Cabosse-700; this suggests that activation promotes a slight crystallization or reorganization of carbon structures. The crystalline phases in the CPH family are linked to the presence of different chemical compounds and composition resulting from the high ash content (see Table 1). The most intense XRD peaks present in the CPH family correspond to the crystalline compounds such as calcium carbonate ($CaCO_3$) at 2θ = 29.35 ° (COD 9007687) for Cabosse-500 and to the potassium carbonate (K_2CO_3) at 2θ = 30.16° (COD 9009645) and 30.06 ° (COD 9010981) for Cabosse-700 and Cabosse-A-700, respectively, with a higher intensity peak observed in the activated biochar. Other crystalline compounds such as potassium sulfate (K_2SO_4), potassium chloride (KCl), silicon dioxide (SiO_2), calcium silicate (Ca_2SiO_4), and magnesium carbonate ($MgCO_3$) are also present, as shown in Figure 5.

3.1.4. TGA Analysis

The conversion of CPH into biochar through pyrolysis and subsequent activation processes involves intricate changes in its moisture, volatile, fixed carbon, and ash content, along with changes in elemental composition, notably carbon and potassium levels. TGA profiles of the CPH family under N_2 and air illustrate varying thermal stabilities (Figure 6), as indicated by Salgado et al. [46]. Pyrolysis at 500 °C results in a significant decrease in moisture from 10.1% to 6.6% and volatile content from 62.6% to 31.7% compared to raw CPH (Figure 6a). This reflects the thermal decomposition of organic matter and the removal of volatile compounds, along with an increase in fixed carbon content from 19.3% to 44.4% and ash content from 8% to 17.3% (Figure 6b). This high ash content is attributed to potassium levels in raw biomass (4.03% [22]). Conversely, pyrolysis at 700 °C leads to further decomposition of volatile organic compounds, reducing moisture (to 1.1%) and volatile content (to 21.3%), possibly due to carbohydrate breakdown at higher pyrolysis temperature [47,48], with an increase in fixed carbon content (to 56.7%). Higher pyrolysis temperatures enhance mineral concentration and destructive volatilization of lignocellulosic matter, explaining the increased ash content, as indicated by Tsai et al. [49]. These findings are consistent with previous research on biochar production from various biomass sources [50,51]. Cabosse-A-700 shows a notable increase in ash content, i.e., 26% compared to 20.9% in Cabosse-700, accompanied by a substantial increase in potassium content from 18% in pyrolyzed biochar to 35% in activated sample (EDX analysis in Table 1). This suggests the incorporation of potassium-rich compounds during activation, contributing to a higher ash content in Cabosse-A-700 compared to its pyrolyzed counterpart.

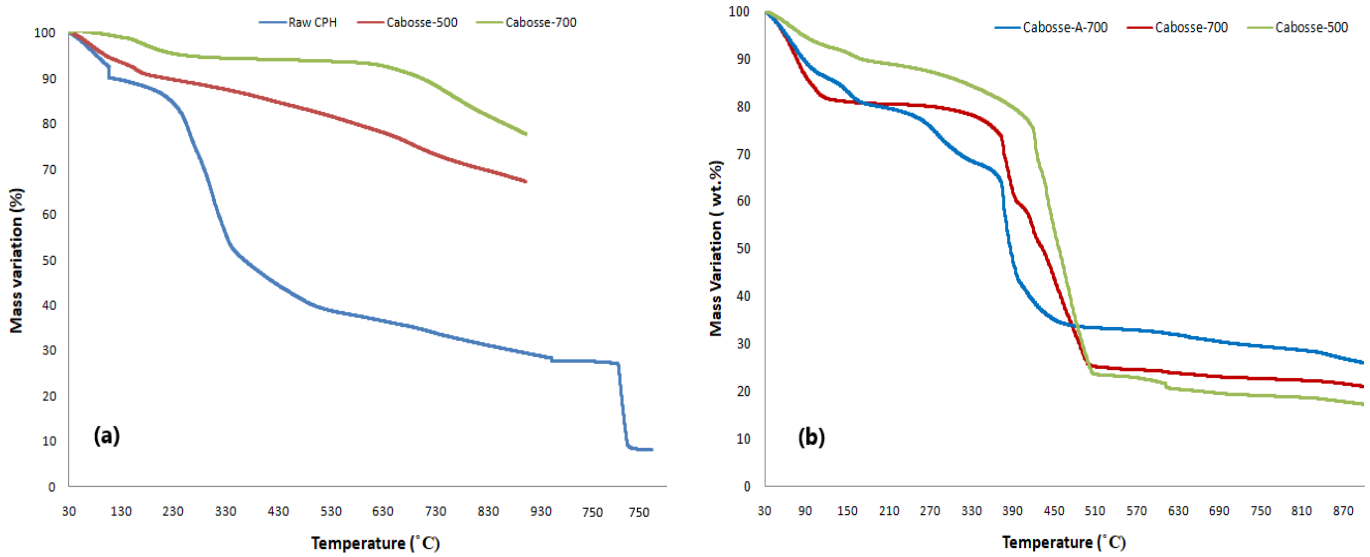

Figure 6. Thermogravimetric analysis curves for the CPH family (**a**) under N_2 for Cabosse-500 and Cabosse-700 and N_2 followed by air for raw CPH, (**b**) under air for Cabosse-500, Cabosse-700, and Cabosse-A-700.

3.1.5. Physical Characterization

The N_2 isotherms of Cabosse-500 and Cabosse-700 showed very low adsorbed volumes (<3.5 $cm^3\ g^{-1}$) (Figure 7a) with reversible desorption, indicating non-porous characteristics (V_t = 0.0002 $cm^3\ g^{-1}$ for Cabosse-500 and 0.003 $cm^3\ g^{-1}$ for Cabosse-700, Table 1), consistent with type II isotherm according to IUPAC classification [52]. However, Cabosse-A-700 exhibited a notable increase in adsorption at P/P_0 < 0.2, indicating micropore filling (type I isotherm), supported by the rise in micropore volume from 0 in Cabosse-700 to 0.011 $cm^3\ g^{-1}$. At higher pressures, the isotherm deviated from the parallel shape with P/P_0, suggesting small mesopores presence (V_{meso} increase from 0.003 (Cabosse-700) to 0.049 $cm^3\ g^{-1}$, Table 1). In a recent study, the N_2 isotherm of a biochar-based CPH produced at 800 °C exhibited both type I (micropores) and type IV (mesopores), showing an improvement in pore properties with the pyrolysis temperature increased from 700 to 800 °C [18]. CO_2 adsorption at 273 K into Cabosse-A-700, as shown in Figure 7b, displayed an initial sharp increase in adsorption without reaching a plateau at high pressure, which indicates the presence of ultra-micropores. Table 1 reveals that CO_2 activation of the pyrolyzed sample increases BET surface area from 41 to 112 $m^2\ g^{-1}$ by CO_2 adsorption and from 4 to 97 $m^2\ g^{-1}$ by N_2 adsorption. As confirmed by the literature, biochar activation improves textural properties [47,53,54]. Additionally, the BET surface area can be further increased by washing away residual K-species. Despite the increase in pyrolysis temperature from 500°C to 700°C, the slight increase in BET surface area by N_2 adsorption (77 K) from 3 $m^2\ g^{-1}$ to 4 $m^2\ g^{-1}$ may relate to the approximate constancy in elemental analysis between Cabosse-500 and Cabosse-700 (Table 1). This result suggests the potential saturation of pore development beyond 500 °C [55]. Since the surface areas of Cabosse-500 and Cabosse-700 are very low (2 and 3 m^2/g, respectively), these values fall within the error and detection limits of the equipment, making it challenging to obtain accurate pore size distribution data. The reason why the BET surface measured by CO_2 adsorption is higher than that measured by N_2 adsorption (77 K) is related to better adsorption of CO_2 into narrower pores due to the higher adsorption temperature (273 K), which allows better diffusion of this gas [56]. In measuring the CO_2 adsorption isotherms, data were collected at pressures below 0.03 P/P_0 to ensure that adsorption occurs primarily within the monolayer region. This method is essential for accurate BET surface area calculations, as it reduces the influence of multilayer adsorption and pore filling.

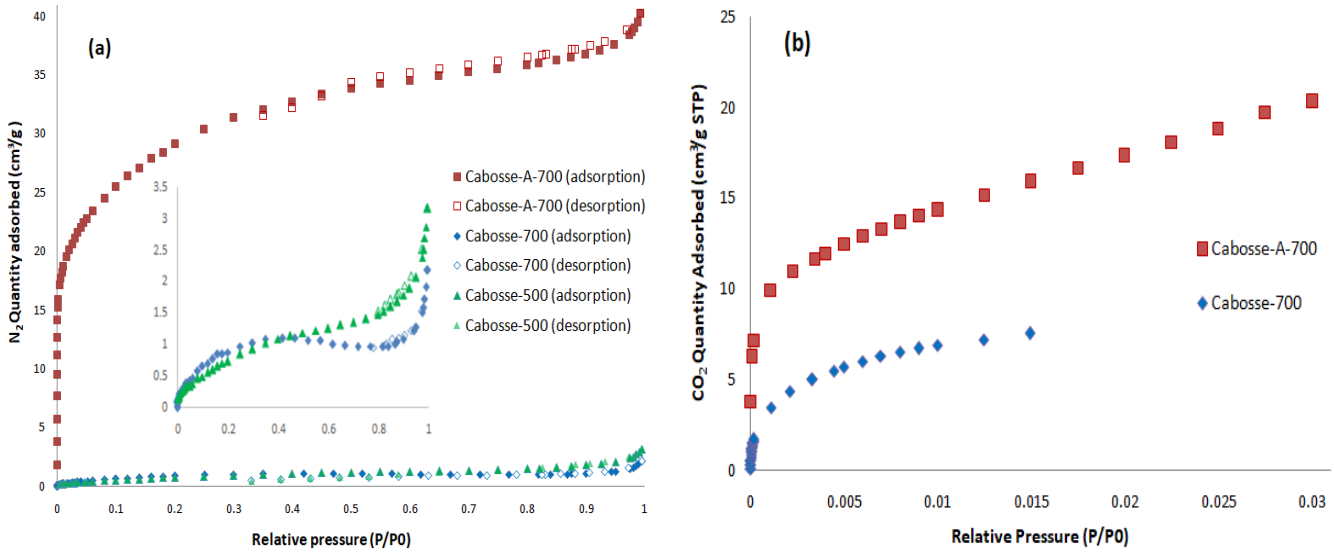

Figure 7. (**a**) Adsorption–desorption isotherm of cabosse family (N_2, 77 K). (**b**) Adsorption isotherm of Cabosse-700 and Cabosse-A-700 (CO_2, 273 K).

Total pore volume increased from 0.0002 to 0.003 $cm^3\ g^{-1}$ by increasing the pyrolysis temperature from 500 °C to 700 °C and further to 0.06 $cm^3\ g^{-1}$ after activation. Both Cabosse-500 and Cabosse-700 exhibit negligible micropore volume, but the mesopore volume increases from 0.0002 to 0.003 $cm^3\ g^{-1}$ (Cabossse-700). Micropores were absent at both pyrolysis temperatures due to pore blockage from condensed organic matter. The same trend was observed by Qiu el al. [57], whose findings showed that the micropore volumes of peanut shell-based biochars are negligible until the pyrolysis temperature reaches 800 °C [57]. However, micropores (<2 nm) and mesopores (between 2 and 50 nm) increased after activation, with V_{micro} from 0 to 0.011 $cm^3\ g^{-1}$ and V_{meso} from 0.003 to 0.049 $cm^3\ g^{-1}$ (Table 1). Thus, activation introduces additional textural changes, creating a more porous material, significantly increasing the surface area accessible for adsorption [47].

3.2. Heat of Adsorption

The differences in the heat of adsorption for the CPH family, Cabosse-500, Cabosse-700, and Cabossse-A-700, are attributed to the changes in their physical and chemical properties (Figure 8). This difference reflects the interaction strength between CO_2 and the adsorbent surface. It was determined by integrating the findings of the CO_2 adsorption isotherms under the pressure ranges and the calorimetry measurements of CO_2 adsorption into the CPH family at 303 K as a function of pressure. The calculated heat of adsorption for the CPH family falls within the range of CO_2 physisorption (<40 kJ mol^{-1}), indicating a reversible adsorption mechanism [58]. The predominant adsorption interactions, primarily governed by physical mechanisms such as Van Der Waals forces, stem from the dipole–dipole interactions [59]. This heat of Cabosse-500, Cabosse-700, and Cabossse-A-700 decreases from 23.02 ± 0.01, 38 ± 1, and 19 ± 1 kJ mol^{-1} to 14 ± 3, 23 ± 4, and 12 ± 3 kJ mol^{-1}, respectively, in a corresponding pressure range of 0.1–2 MPa. The highest heat for the CPH family is in the low-pressure range because gas molecules are more likely to be adsorbed onto accessible active sites on the adsorbent's surface. As pressure rises, it begins to decrease, a common phenomenon in gas–solid adsorption systems because CO_2 molecules compete more for the limited number of active sites, weakening the interactions between the samples and CO_2 [60]. At very high pressure, the heat of adsorption reaches a plateau because most accessible adsorption sites are occupied. The same trend has been consistently observed in recent studies [61–63]. By comparing the heat of adsorption for the CPH family at 0.1 MPa, Cabosse-500 shows a lower value of 23.02 ± 0.01 kJ mol^{-1} than Cabosse-700 (38 ± 1 kJ mol^{-1}), likely due to fewer active sites and lower oxygen content (Table 1). For Cabosse-700, there is an enhancement in the electrostatic interactions between CO_2 and

the surface oxygen groups. However, the heat value of Cabosse-A-700 (19.33 kJ mol^{-1}) is lower than on the studied biochars, suggesting that the activation process likely increases the surface area and porosity and therefore increases the adsorption capacity of CO_2 as confirmed by the adsorption isotherms (see Figure 9). Also, the elevated potassium content in this sample may increase competition for adsorption sites on the material's surface, leading to weaker interactions between CO_2 molecules and the surface and consequently a lower heat of adsorption. Cabosse-A-700 relies predominantly on physical adsorption mechanisms, such as Van der Waals forces, which enhance its efficiency for regeneration.

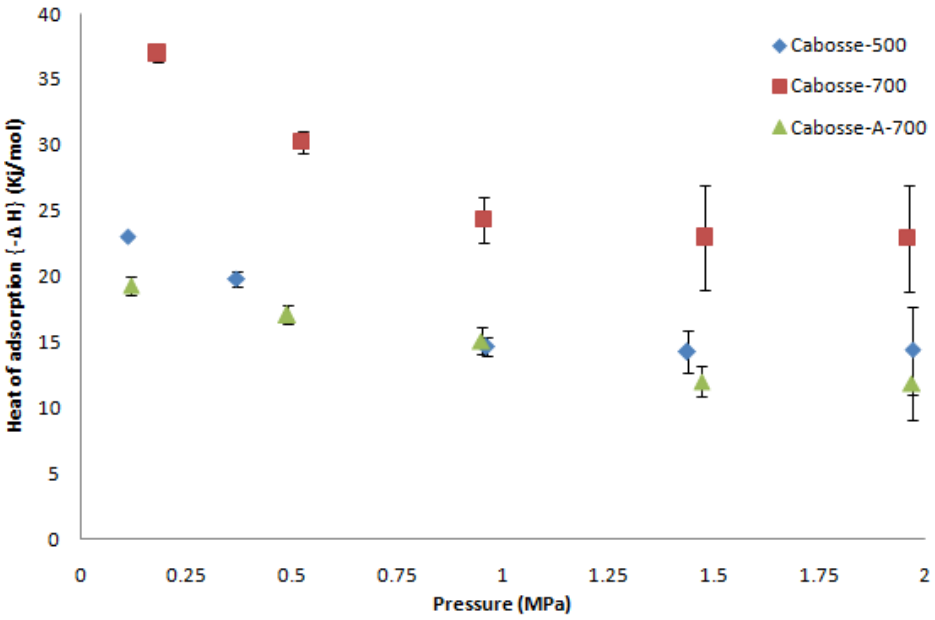

Figure 8. Heat of adsorption of the CPH family at 303 K as a function of pressure.

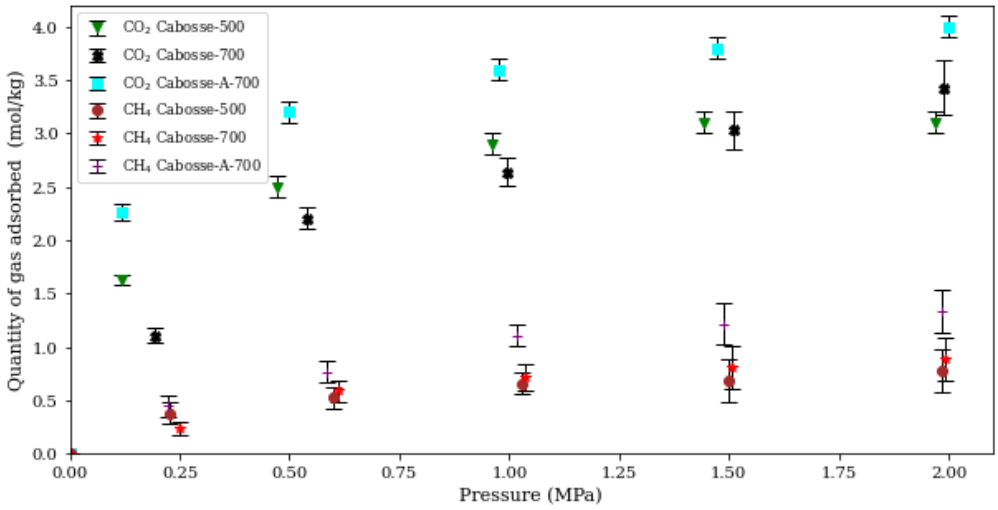

Figure 9. CO_2 and CH_4 adsorption isotherms of the CPH family at 303 K as a function of pressure.

3.3. Adsorption Isotherms

The CPH family, including Cabosse-500, Cabosse-700, and Cabosse-A-700, exhibits a higher affinity to CO_2 compared to CH_4 (Figure 9), primarily due to CO_2 being a polar molecule which enables stronger interactions with the polar or charged sites on the surface of the CPH family. In contrast, CH_4 relies on weaker Van Der Waals forces for adsorption [13,64]. Despite the poor structure of the pyrolyzed samples, their CO_2 adsorption capacities (3.1 $\pm$ 0.1 for Cabosse-500 and 3.4 $\pm$ 0.3 for Cabosse-700) are higher than those

obtained in other studies conducted on biochars, i.e., sawdust pyrolyzed at 450 and 750 °C (0.45 mol kg^{-1} and 1.03 mol kg^{-1}, respectively, at 303 K) [65] and cotton wood pyrolyzed at 600 °C (1.31 mol kg^{-1} at 298 K) [66]. Cabosse-700 has been observed to improve CO_2 adsorption compared to Cabosse-500; this improvement despite the absence of the micropores can be attributed to the development of specific surface sites and the increased quantity of oxygen functionalities as shown by the EDX results (Table 1). These oxygen groups promote hydrogen bonding between CO_2 and the carbon surface.

However, increasing the pyrolysis temperature from 500 to 700 °C has no impact on CH_4 adsorption capacity (Figure 9), indicating no significant change in the structure. This suggests that the ideal pyrolysis temperature for generating an adsorbent with improved surface area and suitable pore structure is about 500 °C, and further temperature increase may not enhance adsorption properties, as confirmed by the nearly constant surface area (Table 1). On the other hand, activation of the biochar at 700 °C improves adsorption capacity for both CO_2 and CH_4 (Figure 9) by increasing surface functionalities, specific surface area, and the formation of micropores and mesopores as shown in Table 1. This leads to more available adsorption sites and improved accessibility for both CO_2 and CH_4 [67,68]. This improvement is attributed to the increase in BET surface area from 4 m^2g^{-1} to 97 m^2g^{-1} and total pore volume from 0.003 to 0.06 cm^3 g^{-1}, as shown in Table 1, which provides more adsorption sites and an optimal structure for CO_2 capture [67–69]. In other words, Cabosse-A-700 exhibits heterogeneous surface properties with bottleneck-shaped pore entrances, largely due to the increase in ash content during activation, from 20.9% in Cabosse-700 to 26% (Table 1) [69]. To optimize the CPH samples for CO_2 capture in biogas upgrading, the focus should be on chemically modifying the samples, particularly by enhancing basic groups (e.g., nitrogen groups) or oxygenated groups such as carboxyl and hydroxyl which improve interactions with CO_2 molecules.

In fact, for the real biogas stream containing water vapor, the high potassium content in Cabosse-A-700 (34.6%, Table 1), primarily in the form of K_2CO_3, facilitates chemical interaction with both CO_2 molecules and water vapor, resulting in kalicinite formation ($KHCO_3$) (Figure 10). XRD analysis post-CO_2 adsorption at low pressure and ambient conditions (air/humidity) storage after three months (Figure 11) confirms the $KHCO_3$ formation (COD 9010981) compared to K_2CO_3 in Cabosse-A-700. This interaction enhances CO_2 capture and improves CO_2/CH_4 separation, enabling Cabosse-A-700 to capture higher quantities of CO_2 from biogas without water vapor separation prior to the upgrading unit [70]. Regarding Cabosse-A-700 regeneration, its heating at 373 K decomposes $KHCO_3$ into K_2CO_3, a reversible reaction when the latter compound is exposed to CO_2 and H_2O, as depicted below [71]:

$$2KHCO_3 <=> K_2CO_3 + CO_2 + H_2O$$

To thoroughly evaluate the reusability of Cabosse-A-700 in practical applications, future research should include experiments under wet conditions and assess the stability of the materials over multiple reaction cycles.

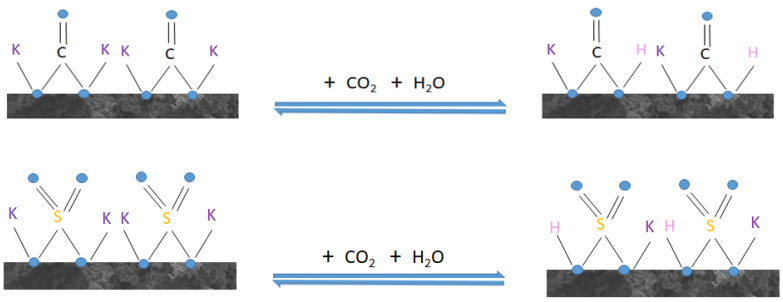

Figure 10. Scheme of CO_2 adsorption on the CPH family in the presence of K_2CO_3 and K_2SO_4 under wet conditions.

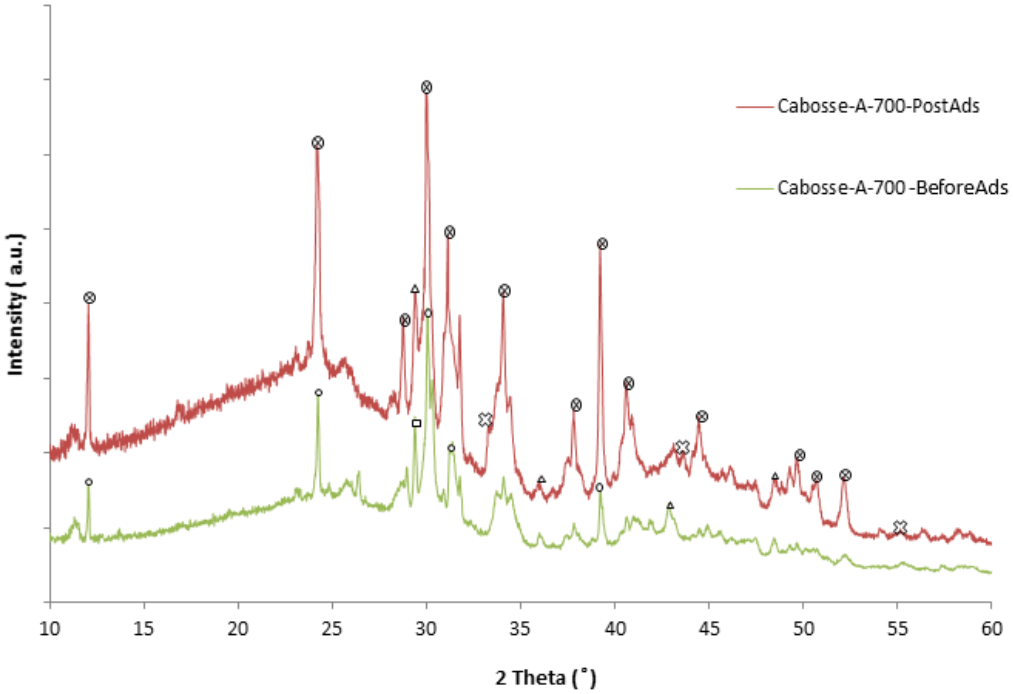

Figure 11. XRD analysis of the activated biochar before and post CO_2 adsorption (after three months) at low pressure and ambient conditions(air/humidity) storage. ⊗ $KHCO_3$, ○ K_2CO_3, △ $CaCO_3$, □ SiO_2, and × $MgCO_3$

3.4. Approximate Adsorption Performance Indicator

The preliminary performance of the CPH family was assessed on the adsorption of the pure CO_2 and CH_4 gases, rather than their binary mixture, using the AAPI relation. Since the primary objective is to separate CO_2 from CH_4, the parameter "adsorption capacity" with an exponent "B = 2" was given higher importance, while the exponents (A and C, see Equation (2)) of the other two parameters were kept at one [35]. The AAPI results indicate that the ideal adsorbent varies with pressure, as shown in Figure 12. Under the very-low-pressure region (<0.5 MPa), Cabosse-A-700 outperforms the other two adsorbents; it has the highest values with a maximum of 2.4 ± 0.1 at 0.1 MPa. This improvement is attributed to the increased specific surface area and the formation of micropores, which enhance the CO_2 adsorption capacity in this region. However, in the intermediate pressure range between 0.5 and 1.25 MPa, AAPI suggests that Cabosse-500 is the most effective adsorbent due to its higher approximate selectivity (between 4.6 ± 0.2 and 5.0 ± 0.1), thanks to its lower CH_4 adsorption capacity and heat of CO_2 adsorption (see Figures 8 and 9). However, in the high-pressure range (>1.25 MPa), Cabosse-A-700 becomes the most effective adsorbent in the CPH family due to its higher CO_2 adsorption capacity and the lowest heat of adsorption, despite its higher CH_4 adsorption capacity (>1.2 ± 0.04) (Figure 9).

It is evident from the data presented in Table 2 that the sequence order of the heat of adsorption of CO_2, the CO_2 working capacity, and the approximate selectivity of CO_2 over CH_4 on the CPH family do not match the order of the AAPI values. This highlights the importance of using the AAPI indicator as an initial evaluation of the performance of adsorbents for separating a binary gas using pure gas adsorption. Thus, it seems that it is unnecessary to activate the biochar if the aim is to separate CO_2 in the moderate pressure range as seen in Figure 12, which lowers the cost of the process on the industrial scale.

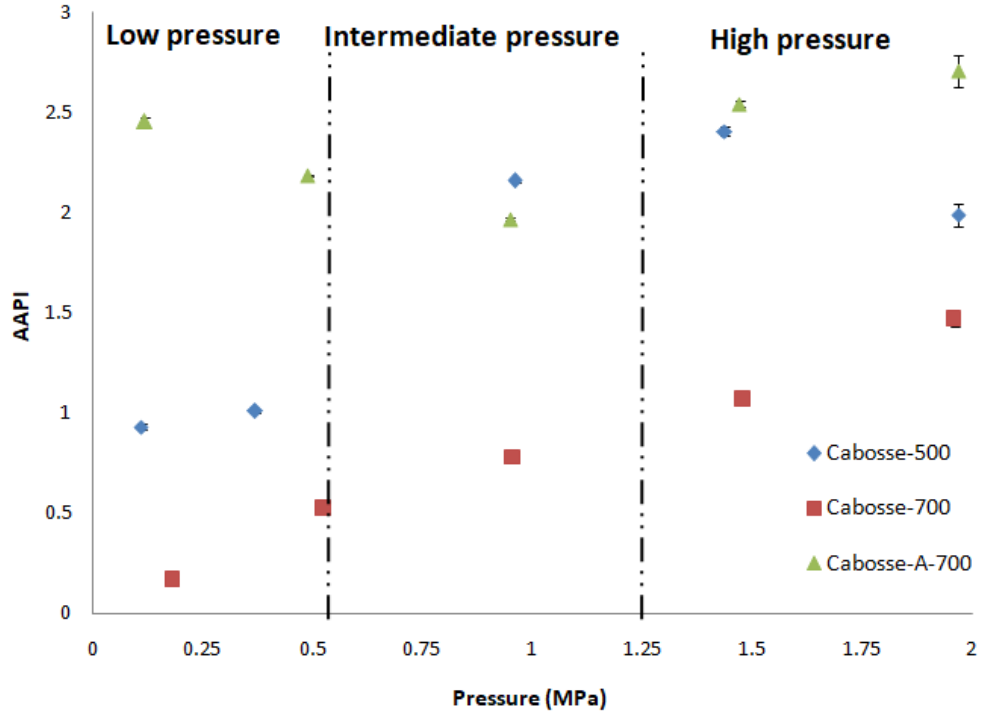

Figure 12. AAPI values of the cabosse family at 303 K as a function of pressure. Uncertainty calculated using the propagation of errors formula.

Table 2. Adsorption parameters for the CPH family used at 303 K and at the two pressures, 0.1 and 1.96 MPa.

	0.1 MPa			1.96 MPa		
	Cabosse-500	**Cabosse-700**	**Cabosse-A-700**	**Cabosse-500**	**Cabosse-700**	**Cabosse-A-700**
n_{CO2} (mol kg^{-1})	1.6 ± 0.1	0.6 ± 0.1	2.3 ± 0.1	3.1 ± 0.1	3.4 ± 0.3	4.0 ± 0.1
n_{CH4} (mol kg^{-1})	0.2 ± 0.1	0.12 ± 0.04	0.2 ± 0.1	0.8 ± 0.2	0.9 ± 0.2	1.3 ± 0.2
$AS(CO_2/CH_4)$	9 ± 1	5.0 ± 0.1	10 ± 1	4 ± 0.1	3.9 ± 0.1	3.00 ± 0.03
$-\Delta H_{CO_2}$ (kJ mol^{-1})	23.02 ± 0.01	38 ± 1	19 ± 1	14 ± 3	23 ± 4	12 ± 3
AAPI	0.93 ± 0.01	0.04 ± 0.02	2.4 ± 0.1	2.0 ± 0.1	1.5 ± 0.1	3.00 ± 0.08

4. Conclusions

This study presents a detailed examination of the physicochemical characteristics and adsorption performance of three cocoa pod husk (CPH) samples: Cabosse-500, Cabosse-700, and Cabosse-A-700. SEM analysis reveals that Cabosse-A-700 possesses a more developed pore structure with extensive cracking compared to Cabosse-700. EDX analysis shows a significant reduction in carbon content in Cabosse-A-700, indicating selective removal of specific carbonaceous components, which enhances its adsorption properties. EDX and DRX analyses identify potassium as a dominant element, mainly in the forms K_2SO_4 and K_2CO_3. The study emphasizes key adsorption parameters, including adsorption isotherms, heat of adsorption, and approximate selectivity, obtained using CO_2 and CH_4 at 303 K, the main components of biogas. Adsorption isotherms show a greater affinity for CO_2 over CH_4, with Cabosse-A-700 exhibiting the highest CO_2 capture performance, attributed to its increased surface area and formation of micro- and mesopores. Even at a pyrolysis temperature of 500 °C, Cabosse-500 captures CO_2 at 3.1 mol kg^{-1}, highlighting the potential of CPH as a cost-effective biochar alternative with CO_2 capture performance comparable to costly adsorbents. The heat of CO_2 adsorption indicates that the CPH family follow a physisorption mechanism, with Cabosse-700 exhibiting higher initial values due to its higher oxygen content, which enhances interaction energy between the surface and CO_2

molecules. Additionally, a new indicator, the Adsorbent Performance Indicator (AAPI), is used to evaluate the adsorbents based on their adsorption parameters. This indicator shows that Cabosse-A-700 outperforms the other samples under both low- and high-pressure conditions due to its improved structure and superior CO_2 capture capacity. Significantly, the study demonstrates that activation is unnecessary for CO_2 separation at moderate pressures, potentially lowering industrial costs. Overall, Cabosse-A-700 emerges as the most promising candidate for CO_2 separation from biogas mixtures, offering a cost-effective solution for biogas upgrading.

Author Contributions: Conceptualization , K.A.A.; methodology, K.A.A., C.M.G., C.V. and J.-M.L.M.; validation, K.A.A., C.H., C.M.G. and V.P.; formal analysis, K.A.A., C.M.G., C.V., J.-M.L.M. and L.T.; investigation, K.A.A., C.M.G., C.V., J.-M.L.M., J.A.C. and L.M.; resources, C.M.G., J.-M.L.M., C.V., C.H., D.C.M.-S. and D.P.; writing—original draft preparation, K.A.A.; writing—review and editing, C.H. and C.M.G.; visualization, K.A.A.; supervision, C.H., V.P. and C.M.G.; funding acquisition, C.H. and D.P. All authors have read and agreed to the published version of the manuscript.

Funding: This research was carried under the framework of E2S UPPA supported by the "Investissements d'Avenir" French programme managed by ANR (Agence Nationale de la recherche (France)) (ANR-16-IDEX-0002). Financial support for the BioCad project is gratefully acknowledged.

Data Availability Statement: Data are contained within the article.

Acknowledgments: The authors thank Gautier Schrodj (for TGA analyses) and Adrian Beda (for SEM and EDX analyses) via IS2M technical platforms. Scientific exchange activities between Colombia and France were supported by Ecosnord (France) and Minciencias (Colombia).

Conflicts of Interest: The authors declare no conflicts of interest.

Abbreviations

The following abbreviations are used in this manuscript:

CPH	Cocoa Pod Husk
CO_2	Carbon dioxide
CH_4	Methane
N_2	Nitrogen
PSA	Pressure Swing Adsorption
AAPI	Approximate Adsorption Performance Indicator
IUPAC	International Union of Pure and Applied Chemistry
TGA	Thermogravimetric Analysis
EDX	Energy Dispersive X-ray
XRD	X-ray Diffraction (XRD)
SEM	Scanning Electron Microscopy
BET	Brunauer-Emmett-Teller

Appendix A

Appendix A.1

Raw biomass preparation: Cocoa trees were randomly chosen within the production unit; harvesting, grain separation, and CPH removal followed the FEDECACAO methodology. Subsequently, the harvested pods were transported to the Technological University of Pereira where they were selected, uniformly cut, and cleaned with 3% hypochlorite solution. The prepared samples were then dried in a Thermo Scientific natural convection oven (Ref. 5108112) for 48 to 60 h at 65 °C until a constant weight was achieved. CPH is composed of three layers: epicarp, mesocarp, and endocarp, which constitute the outer, middle, and inner pericarp. It is a lignocellulosic material composed mainly of cellulose (18.4–44.7%), hemicellulose (10.0–38.1%), lignin (19.7–34.8%), pectins (6.0–12.6%), oils, and waxes [72].

Appendix A.2

Activated biochar preparation: Attempts to activate Cabosse-700 with CO_2 at 900 °C and 800 °C for 60 min at a flow rate of 12 L h^{-1} were unsuccessful due to complete burning of the sample, likely attributed to the high potassium content (18.1%), which can act as a chemical agent during physical activation and catalyze reactions in the presence of CO_2 at high temperatures (>700 °C) [73,74]. Finally, activation at a lower temperature of 700 °C for 1 h at a CO_2 flow rate of 6 L h^{-1} yielded Cabosse-A-700 with a mass loss of 8.6%.

Appendix A.3

Protocol for the gas adsorption isotherm experiment: The apparatus used to obtain the pure gas adsorption isotherms is a homemade high-pressure manometric setup represented schematically in Figure 3. The system's key components are the dosing cell, the adsorption cell, and the piezoresistive Keller pressure regulator type PAA-33X (with 0.05% uncertainty from vacuum to 3.3 MPa) connected to the dosing volume. To maintain the isothermal conditions of the apparatus, the entire system was placed into a bath of water continuously heated at about 303 K with a Lauda model water bath circulator heater, with two thermocouples fixed in the two cells and in the water bath to shield it from the isothermal conditions. The various components were separated using valves to limit the "dead space" volume. First, the entire apparatus was placed under vacuum pressure (10^{-2} Pa) for a 24 h outgassing phase at 373 K, and then the study temperature (303 K) for the adsorption isotherm was settled. The accessible volume in the adsorption cell is determined by successive helium expansions from the dose volume (V_d) to the adsorption volume ($V_{\mathbf{ads}}$) using the gas equation of state; to remove all traces of helium, the system is vacuumed for 4 h. After that, a quantity of pure gases (CH_4 or CO_2) is introduced into the dosing cell via valve V_1, and the pressure is registered when the equilibrium is reached (constant pressure). The gas is then expanded into the adsorption cell by opening valves V_2 and V_4, and the pressure is registered when the equilibrium is achieved. An accumulative method was chosen to carry out the adsorption isotherm, with an increase in pressure of ≈5 bar between each measurement.

References

1. Guo, M.; Song, W.; Buhain, J. Bioenergy and biofuels: History, status, and perspective. *Renew. Sustain. Energy Rev.* **2015**, *42*, 712–725. [CrossRef]
2. Bharathiraja, D.; Sudharsana, T.; Jayamuthunagai, J.; Ramanujam, P.K.; Sivasankaran, C.; Iyyappan, J. Biogas production—A review on composition, fuel properties, feed stock and principles of anaerobic digestion. *Renew. Sustain. Energy Rev.* **2018**, *90*, 570–582. [CrossRef]
3. Jiang, X.; Sommer, S.G.; Christensen, K.V. A review of the biogas industry in China. *Energy Policy* **2011**, *39*, 6073–6081. [CrossRef]
4. Aghel, B.; Behaein, S.; Alobaid, F. CO_2 capture from biogas by biomass-based adsorbents: A review. *Fuel* **2022**, *328*, 125276. [CrossRef]
5. Sahota, S.; Shah, G.; Ghosh, P.; Kapoor, R.; Sengupta, S.; Singh, P.; Vijay, V.; Sahay, A.; Vijay, V.K.; Thakur, I.S. Review of trends in biogas upgradation technologies and future perspectives. *Bioresour. Technol. Rep.* **2018**, *1*, 79–88. [CrossRef]
6. Awe, O.W.; Zhao, Y.; Nzihou, A.; Minh, D.P.; Lyczko, N. A Review of Biogas Utilisation, Purification and Upgrading Technologies. *Waste Biomass Valorization* **2017**, *8*, 267–283. [CrossRef]
7. Sun, Q.; Li, H.; Yan, J.; Liu, L.; Yu, Z.; Yu, X. Selection of appropriate biogas upgrading technology-a review of biogas cleaning, upgrading and utilisation. *Renew. Sustain. Energy Rev.* **2015**, *51*, 521–532. [CrossRef]
8. Canevesi, R.L.S.; Andreassen, K.A.; da Silva, E.A.; Borba, C.E.; Grande, C.A. Pressure Swing Adsorption for Biogas Upgrading with Carbon Molecular Sieve. *Ind. Eng. Chem. Res.* **2018**, *57*, 8057–8067. [CrossRef]
9. Patterson, H.B.W. Chapter 2—Adsorption. In *Bleaching and Purifying Fats and Oils*, 2nd ed.; List, G.R., Ed.; AOCS Press: Champaign, IL, USA, 2009; pp. 53–67. [CrossRef]
10. Bedia, J.; Peñas-Garzón, M.; Gómez-Avilés, A.; Rodriguez, J.J.; Belver, C. Review on Activated Carbons by Chemical Activation with FeCl3. *C* **2020**, *6*, 21. [CrossRef]
11. Ioannidou, O.; Zabaniotou, A. Agricultural residues as precursors for activated carbon production—A review. *Renew. Sustain. Energy Rev.* **2007**, *11*, 1966–2005. [CrossRef]
12. Kumar, A.; Bhattacharya, T.; Shaikh, W.A.; Roy, A.; Chakraborty, S.; Vithanage, M.; Biswas, J.K. Multifaceted applications of biochar in environmental management: A bibliometric profile. *Biochar* **2023**, *5*, 11. [CrossRef]

13. Peredo-Mancilla, D.; Ghimbeu, C.; Réty, B.; Ho, B.N.; Perez, D.; Vaulot, C.; Hort, C.; Bessieres, D. Surface-Modified Activated Carbon with a Superior CH_4/CO_2 Adsorption Selectivity for the Biogas Upgrading Process. *Ind. Eng. Chem. Res.* **2022**, *61*, 12710–12727. [CrossRef]
14. Bedia, J.; Peñas-Garzón, M.; Gómez-Avilés, A.; Rodriguez, J.J.; Belver, C. A Review on the Synthesis and Characterization of Biomass-Derived Carbons for Adsorption of Emerging Contaminants from Water. *C* **2018**, *4*, 63. [CrossRef]
15. Vísquez, Z.S.; de Carvalho Neto, D.P.; Pereira, G.V.M.; Vandenberghe, L.P.S.; de Oliveira, P.Z.; Tiburcio, P.B.; Rogez, H.L.G.; Ges Neto, A.; Soccol, C.R. Biotechnological approaches for cocoa waste management: A review. *Waste Manag.* **2019**, *90*, 72–83. [CrossRef]
16. Hernández-Mendoza, A.G.; Saldaa-Trinidad, S.; Mart¡nez-Hernández, S.; Prez-Sariana, B.Y.; Líinez, M. Optimization of alkaline pretreatment and enzymatic hydrolysis of cocoa pod husk (*Theobroma cacao* L.) Ethanol Prod. *Biomass Bioenergy* **2021**, *154*, 106268. [CrossRef]
17. Federación Nacional de Cacaoteros de Colombia. *Caracterización fisícoquímica y beneficio del grano de cacao (Theobroma cacao L.) en Colombia.*; Federacion Nacional de Cacaoteros— FEDECACAO: Bogotá, Colombia, 2005.
18. Tsai, W.T.; Hsu, C.H.; Lin, Y.Q.; Tsai, C.H.; Chen, W.S.; Chang, Y.T. Enhancing the Pore Properties and Adsorption Performance of Cocoa Pod Husk (CPH)-Derived Biochars via Post-Acid Treatment. *Processes* **2020**, *8*, 144. [CrossRef]
19. de Oliveira, P.Z.; de Souza Vandenberghe, L.P.; Rodrigues, C.; de Melo Pereira, G.V.; Soccol, C.R. Exploring cocoa pod husks as a potential substrate for citric acid production by solid-state fermentation using *Aspergillus Niger* Mutant Strain. *Process Biochem.* **2022**, *113*, 107–112. [CrossRef]
20. Gallego, A.M.; Zambrano, R.A.; Zuluaga, M.; Camargo Rodríguez, A.V.; Candamil Cortés, M.S.; Romero Vergel, A.P.; Arboleda Valencia, J.W. Analysis of fruit ripening in *Theobroma Cacao* Pod Husk Based Untargeted Metabolomics. *Phytochemistry* **2022**, *203*, 113412. [CrossRef]
21. Meza-sepulveda, D.C.; Castro, A.M.; Zamora, A.; Arboleda, J.W.; Gallego, A.M.; Camargo-Rodr¡guez, A.V. Bio-Based Value Chains Potential in the Management of Cacao Pod Waste in Colombia, a Case Study. *Agronomy* **2021**, *11*, 693. [CrossRef]
22. Tsai, C.H.; Tsai, W.T.; Liu, S.C.; Lin, Y.Q. Thermochemical characterization of biochar from cocoa pod husk prepared at low pyrolysis temperature. *Biomass Convers. Biorefinery* **2018**, *8*, 1–7. [CrossRef]
23. Miles, T.R.; Rasmussen, E.M.; Gray, M. Aqueous Contaminant Removal and Stormwater Treatment Using Biochar. In *Agricultural and Environmental Applications of Biochar: Advances and Barriers*; John Wiley & Sons, Ltd.: Hoboken, NJ, USA, 2016; pp. 341–376.
24. Tsai, W.T.; Jiang, T.J.; Lin, Y.Q. Conversion of de-ashed cocoa pod husk into high-surface-area microporous carbon materials by CO_2 physical activation. *J. Mater. Cycles Waste Manag.* **2019**, *21*, 308–314. [CrossRef]
25. Araoye, A.O.; Agboola, O.S.; Bello, O.S. Insights into chemically modified cocoa pods for enhanced removal of an anti-malaria drug. *Chem. Data Collect.* **2021**, *36*, 100775. [CrossRef]
26. Eletta, O.; Adeniyi, A.; Ighalo, J.O.; Onifade, D.; Ayandele, F. Valorisation of Cocoa (Theobroma cacao) pod husk as precursors for the production of adsorbents for water treatment. *Environ. Technol.* **2020**, *9*, 20–36. [CrossRef]
27. Mansur, D.; Tago, T.; Masuda, T.; Abimanyu, H. Conversion of cacao pod husks by pyrolysis and catalytic reaction to produce useful chemicals. *Biomass Bioenergy* **2014**, *66*, 275–285. [CrossRef]
28. Chatterjee, R.; Sajjadi, B.; Chen, W.Y.; Mattern, D.L.; Hammer, N.; Raman, V.; Dorris, A. Effect of Pyrolysis Temperature on PhysicoChemical Properties and Acoustic-Based Amination of Biochar for Efficient CO_2 Adsorption. *Front. Energy Res.* **2020**, *8*, 85. [CrossRef]
29. Zhang, T.; Walawender, W.P.; Fan, L.T.; Fan, M.; Daugaard, D.; Brown, R.C. Preparation of activated carbon from forest and agricultural residues through CO_2 activation. *Chem. Eng. J.* **2004**, *105*, 53–59. [CrossRef]
30. Beda, A.; Escamilla-Pérez, A.M.; Simonin, L.; Matei Ghimbeu, C. Vegetal-Extracted Polyphenols as a Natural Hard Carbon Anode Source for Na-Ion Batteries. *ACS Appl. Energy Mater.* **2022**, *5*, 4774–4787. [CrossRef]
31. Abou Alfa, K.; Peredo-Mancilla, D.; Platel, V.; Hort, C. Evaluation of the Performance of an Activated Carbon's Family for Biogas Upgrading Using the Adsorption Performance Indicator. In *Trends in Clean Energy Research, Proceedings of the 9th International Conference on Advances on Clean Energy Research (ICACER 2024), Lille, France, 27–29 April 2024*; Springer: Cham, Switzerland, 2024; pp. 91–99. [CrossRef]
32. Peredo-Mancilla, D.; Ghouma, I.; Hort, C.; Ghimbeu, C.M.; Jeguirim, M.; Bessieres, D. CO_2 and CH_4 Adsorption Behavior of Biomass-Based Activated Carbons. *Energies* **2018**, *11*, 3136. [CrossRef]
33. Ho, B.; Perez, D.; Peredo-Mancilla, D.; Diaz, J.; Hort, C.; Bessieres, D.; Ghimbeu, C. Determination of methane, ethane and propane on activated carbons by experimental pressure swing adsorption method. *J. Nat. Gas Sci. Eng.* **2021**, *95*, 104124. [CrossRef]
34. Iragena Dushime, G.; Bachelart, J.; Abou Alfa, K.; Ghimbeu, C.; Hort, C.; Platel, V. New Promising Modified Activated Carbons for CH_4 and CO_2 Adsorption; In *Environmental Science and Engineering, Proceedings of the 2022 4th International Conference on Environment Sciences and Renewable Energy, Chengdu, China, 27–29 May 2022*; Springer: Berlin/Heidelberg, Germany, 2022.
35. Wiersum, A.D.; Chang, J.S.; Serre, C.; Llewellyn, P.L. An Adsorbent Performance Indicator as a First Step Evaluation of Novel Sorbents for Gas Separations: Application to MetalOrganic Frameworks. *Langmuir* **2013**, *29*, 3301–3309. [CrossRef]
36. He, Z.; Wang, K. The 'ideal selectivity' vs 'true selectivity' for permeation of gas mixture in nanoporous membranes. *IOP Conf. Ser. Mater. Sci. Eng.* **2018**, *323*, 012002. [CrossRef]

37. Asif, K.; Lock, S.S.M.; Taqvi, S.A.A.; Jusoh, N.; Yiin, C.L.; Chin, B.L.F.; Loy, A.C.M. A Molecular Simulation Study of Silica/Polysulfone Mixed Matrix Membrane for Mixed Gas Separation. *Polymers* **2021**, *13*, 2199. [CrossRef] [PubMed]
38. Villota, S.; Lei, H.; Villota, E.; Qian, M.; Lavarias, J.; Taylan, V.; Agulto, I.; Mateo, W.; Valentin, M.; Denson, M. Microwave-Assisted Activation of Waste Cocoa Pod Husk by H_3PO_4 and KOH-Comparative Insight into Textural Properties and Pore Development. *ACS Omega* **2019**, *4*, 7088–7095. [CrossRef]
39. Ahmed, A.S.; Alsultan, M.; Sabah, A.A.; Swiegers, G.F. Carbon Dioxide Adsorption by a High-Surface-Area Activated Charcoal. *J. Compos. Sci.* **2023**, *7*, 179. [CrossRef]
40. Lehmann, J.; Joseph, S. *Biochar for Environmental Management: Science, Technology and Implementation*; Routledge: Boca Raton, FL, USA, 2015.
41. Steiner, C. Considerations in Biochar Characterization. In *Agricultural and Environmental Applications of Biochar: Advances and Barriers*; John Wiley & Sons, Ltd.: Hoboken, NJ, USA, 2016; pp. 87–100.
42. Santhosh, C.; Daneshvar, E.; Tripathi, K.M.; Baltrùnas, P.; Kim, T.; Baltrùnaitù, E.; Bhatnagar, A. Synthesis and characterization of magnetic biochar adsorbents for the removal of Cr(VI) and Acid orange 7 dye from aqueous solution. *Environ. Sci. Pollut. Res.* **2020**, *27*, 32874–32887. [CrossRef]
43. Côrtes, L.; Druzian, S.; Streit, A.; Cadaval, T.; Collazzo, G.; Dotto, G. Preparation of carbonaceous materials from pyrolysis of chicken bones and its application for fuchsine adsorption. *Environ. Sci. Pollut. Res.* **2019**, *26*, 28574–28583. [CrossRef]
44. Katuwal, S.; Ashworth, A.J.; Rafsan, N.A.S.; Kolar, P. Characterization of Poultry Litter Biochar and Activated Biochar as a Soil Amendment for Valorization. *Biomass* **2022**, *2*, 209–223. [CrossRef]
45. Thue, P.S.; Lima, D.R.; Lima, E.C.; Teixeira, R.A.; dos Reis, G.S.; Dias, S.L.P.; Machado, F.M. Comparative studies of physicochemical and adsorptive properties of biochar materials from biomass using different zinc salts as activating agents. *J. Environ. Chem. Eng.* **2022**, *10*, 107632. [CrossRef]
46. Salgado, M.; Abioye, A.; Junoh, M.; Santos, J.; Ani, F. Preparation of activated carbon from babassu endocarpunder microwave radiation by physical activation. *IOP Conf. Ser. Earth Environ. Sci.* **2018**, *105*, 012116. [CrossRef]
47. Park, J.; Hung, I.; Gan, Z.; Rojas, O.J.; Lim, K.H.; Park, S. Activated carbon from biochar: Influence of its physicochemical properties on the sorption characteristics of phenanthrene. *Bioresour. Technol.* **2013**, *149*, 383–389. [CrossRef]
48. Palniandy, L.K.; Yoon, L.W.; Wong, W.Y.; Yong, S.T.; Pang, M.M. Application of Biochar Derived from Different Types of Biomass and Treatment Methods as a Fuel Source for Direct Carbon Fuel Cells. *Energies* **2019**, *12*, 2477. [CrossRef]
49. Tsai, W.T.; Liu, S.C.; Chen, H.R.; Chang, Y.M.; Tsai, Y.L. Textural and chemical properties of swine-manure-derived biochar pertinent to its potential use as a soil amendment. *Chemosphere* **2012**, *89*, 198–203. [CrossRef] [PubMed]
50. Usman, A.R.A.; Abduljabbar, A.; Vithanage, M.; Ok, Y.S.; Ahmad, M.; Ahmad, M.; Elfaki, J.; Abdulazeem, S.S.; Al-Wabel, M.I. Biochar production from date palm waste: Charring temperature induced changes in composition and surface chemistry. *J. Anal. Appl. Pyrolysis* **2015**, *115*, 392–400. [CrossRef]
51. Elnour, A.Y.; Alghyamah, A.A.; Shaikh, H.M.; Poulose, A.M.; Al-Zahrani, S.M.; Anis, A.; Al-Wabel, M.I. Effect of Pyrolysis Temperature on Biochar Microstructural Evolution, Physicochemical Characteristics, and Its Influence on Biochar/Polypropylene Composites. *Appl. Sci.* **2019**, *9*, 1149. [CrossRef]
52. Donohue, M.; Aranovich, G. Classification of Gibbs adsorption isotherms. *Adv. Colloid Interface Sci.* **1998**, *76*, 137–152. [CrossRef]
53. Chen, B.; Chen, Z. Sorption of naphthalene and 1-naphthol by biochars of orange peels with different pyrolytic temperatures. *Chemosphere* **2009**, *76*, 127–133. [CrossRef]
54. Chun, Y.; Sheng, G.; Chiou, G.; Xing, B. Compositions and sorptive properties of crop residue-derived chars. *Environ. Sci. Technol.* **2004**, *38*, 4649–4655. [CrossRef]
55. Chen, Y.; Zhang, X.; Chen, W.; Yang, H.; Chen, H. The structure evolution of biochar from biomass pyrolysis and its correlation with gas pollutant adsorption performance. *Bioresour. Technol.* **2017**, *246*, 101–109. [CrossRef]
56. Beda, A.; Vaulot, C.; Ghimbeu, C.M. Hard carbon porosity revealed by the adsorption of multiple gas probe molecules (N_2, Ar, CO_2, O_2 and H_2). *J. Mater. Chem. A* **2021**, *9*, 937–943. [CrossRef]
57. Qiu, T.; Li, C.; Guang, M.; Zhang, Y. Porous carbon material production from microwave-assisted pyrolysis of peanut shell. *Carbon Res.* **2023**, *2*, 45. [CrossRef]
58. Rashidi, N.A.; Yusup, S.; Lam, H.L. Kinetic Studies on Carbon Dioxide Capture using Activated Carbon. *Chem. Eng. Trans.* **2013**, *35*, 361–366. [CrossRef]
59. Gunawan, T.; Wijiyanti, R.; Widiastuti, N. Adsorption-desorption of CO_2 on zeolite-Y-templated carbon at various temperatures. *RSC Adv.* **2018**, *8*, 41594–41602. [CrossRef] [PubMed]
60. Singh, V.K.; Anil Kumar, E. Measurement and analysis of adsorption isotherms of CO_2 on activated carbon. *Appl. Therm. Eng.* **2016**, *97*, 77–86. [CrossRef]
61. Li, D.; Zhou, J.; Wang, Y.; Tian, Y.; Wei, L.; Zhang, Z.; Qiao, Y.; Li, J. Effects of activation temperature on densities and volumetric CO_2 adsorption performance of alkali-activated carbons. *Fuel* **2019**, *238*, 232–239. [CrossRef]
62. Geng, Z.; Xiao, Q.; Lv, H.; Li, B.; Wu, H.B.; Lu, Y.; Zhang, C. One-Step Synthesis of Microporous Carbon Monoliths Derived from Biomass with High Nitrogen Doping Content for Highly Selective CO_2 Capture. *Sci. Rep.* **2016**, *6*, 30049. [CrossRef]
63. He, J.; Mei, J.; Bao, Z.; Wilcox, J. Facile Synthesis of Nitrogen-doped Porous Carbon for Selective CO_2 Capture. *Energy Procedia* **2014**, *63*, 2144–2151. [CrossRef]

64. Álvarez Gutiérrez, N.; Gil, M.V.; Rubiera, F.; Pevida, C. Adsorption performance indicators for the CO_2/CH_4 separation: Application to biomass-based activated carbons. *Fuel Process. Technol.* **2016**, *142*, 361–369. [CrossRef]
65. Madzaki, H.; KarimGhani, W.A.W.A.B.; NurZalikhaRebitanim; AzilBahariAlias. Carbon Dioxide Adsorption on Sawdust Biochar. *Procedia Eng.* **2016**, *148*, 718–725. [CrossRef]
66. Creamer, A.E.; Gao, B.; Wang, S. Carbon dioxide capture using various metal oxyhydroxide-biochar composites. *Chem. Eng. J.* **2016**, *283*, 826–832. [CrossRef]
67. Zhang, X.; Zhang, S.; Yang, H.; Feng, Y.; Chen, Y.; Wang, X.; Chen, H. Nitrogen enriched biochar modified by high temperature CO_2-ammonia treatment: Characterization and adsorption of CO_2. *Chem. Eng. J.* **2014**, *257*, 20–27. [CrossRef]
68. Zhang, X.; Wu, J.; Yang, H.; Shao, J.; Wang, X.; Chen, Y.; Zhang, S.; Chen, H. Preparation of nitrogen-doped microporous modified biochar by high temperature CO_2-NH_3 treatment for CO_2 adsorption: Effects of temperature. *RSC Adv.* **2016**, *6*, 98157–98166. [CrossRef]
69. Khuong, D.A.; Nguyen, H.N.; Tsubota, T. Activated carbon produced from bamboo and solid residue by CO_2 activation utilized as CO_2 adsorbents. *Biomass Bioenergy* **2021**, *148*, 106039. [CrossRef]
70. Durín, I.; ülvarez Gutirrez, N.; Rubiera, F.; Pevida, C. Biogas purification by means of adsorption on pine sawdust-based activated carbon: Impact of water vapor. *Chem. Eng. J.* **2018**, *353*, 197–207. [CrossRef]
71. Schultz, H.; Bauer, G.; Schachl, E.; Hagedorn, F.; Schmittinger, P. Potassium Compounds. In *Ullmann's Encyclopedia of Industrial Chemistry*; John Wiley & Sons, Ltd.: Hoboken, NJ, USA, 2000. [CrossRef]
72. Ouattara, Y.; Kouadio, E.; Kouassi, E.; Doudjo, S.; Soro, Y.; Yao, B.; Adouby, K.; Drogui, A.; Tyagi, D.; Aina, P. Cocoa pod husk: A review. *Bioresources* **2021**, *16*, 1988–2020. [CrossRef]
73. Kim, J.; Lee, G.; Park, J.E.; Kim, S.H. Limitation of K_2CO_3 as a Chemical Agent for Upgrading Activated Carbon. *Processes* **2021**, *9*, 1000. [CrossRef]
74. Wang, L.; Sun, F.; Hao, F.; Qu, Z.; Gao, J.; Liu, M.; Wang, K.; Zhao, G.; Qin, Y. A green trace K_2CO_3 induced catalytic activation strategy for developing coal-converted activated carbon as advanced candidate for CO_2 adsorption and supercapacitors. *Chem. Eng. J.* **2020**, *383*, 123205. [CrossRef]